8.9 CLOUD RADIATIVE FORCING DURING FIRE ACE USING AVHRR DATA

D. R. Doelling, C. Venkatesan, D. A. Spangenberg
Analytical Services & Materials Inc., Hampton, VA

P. Minnis
Atmospheric Sciences Division, NASA-Langley Research Center, Hampton, VA

1. INTRODUCTION

Clouds have a significant impact on the Arctic radiation budget. Changing ice surface albedos over time diminish or increase the radiative effects of clouds and make it a challenge to detect clouds using satellite data. Atmospheric conditions in the Arctic do not often meet the satellite retrieval assumptions that clouds are colder and brighter than the surface. Therefore, cloud radiative forcing in the Arctic is not well determined from satellite data. Establishing its sign and seasonal variability is critical for assessing the role of clouds in the Arctic climate. Satellite data taken during the First ISCCP Regional Experiment (FIRE) Arctic Clouds Experiment (ACE) are carefully analyzed to provide a more accurate determination of cloud forcing than heretofore possible. Advanced Very High Resolution Radiometer (AVHRR) onboard the NOAA-12 and NOAA-14 spacecraft were determined to be either clear or cloudy at the 1-km pixel level. Thresholds were determined using the 0.65-μm reflectances, the 11.0-μm temperature, and the differences between the 3.75 and 11.0-μm and the 12.0 and 11.0-μm temperatures. Similar thresholds were also determined for the NOAA-15 AVHRR pixels that have replaced the 3.7-μm channel during the day.

No broadband satellite measurements were available during FIRE-ACE (May-July 1998) over the Arctic. Thus, broadband shortwave (0.2 to 5.0-μm) albedo and Outgoing Longwave Radiation (OLR; 5 to 50-μm) were estimated from narrowband AVHRR radiances using empirical narrowband to broadband relationships derived from historical coincident and collocated Earth Radiation Budget Experiment (ERBE) fluxes and NOAA-9 AVHRR data. These AVHRR-derived broadband fluxes have been validated against C-130 Total Solar Broadband Radiometer (TSBR) fluxes taken during the FIRE-ACE experiment. The albedo and OLR are computed for clear and cloudy conditions to estimate cloud forcing. Monthly cloud forcing statistics are determined over a grid near the ship site and correlated with ship instrument measurements. AVHRR also has good temporal sampling enabling an estimate of the diurnal cycle of the cloud radiative forcing.

* Corresponding Author Address: D. R. Doelling, AS&M, Inc., 1 Enterprise Parkway Hampton, VA 23666;
e-mail: d.r.doelling@larc.nasa.gov.

2. NARROWBAND AVHRR DATA

NOAA-12 and NOAA-14 AVHRR High-Resolution Picture Transmission (HRPT) 1-km images were collected during FIRE-ACE. The images were centered on the Surface Heat Budget of the Arctic Ocean (SHEBA) ship and were 600 lines by 1300 elements including the domain between 72°N to 80°N and 180°W to 150°W. This set of images provides good diurnal sampling except for 2000 to 2400 local time.

The visible channel (0.65-μm) counts are converted to narrowband visible radiance L_v using the Rao and Chen (1996 and update 1998) degradation equations for NOAA-14. The NOAA-12 visible counts were normalized to the NOAA-14 counts during the FIRE-ACE period using collocated data over the Arctic. The resulting normalization is

$$C_{N14} = 1.025C_{N12} + 2.88, \qquad (1)$$

where the 10-bit NOAA-12 and 14 counts are C_{N12} and C_{N14},respectively. Thus, the Rao and Chen calibration could be applied to the NOAA-12 data also.

The narrowband VIS albedo is

$$\alpha_v = \pi L_v / [\delta(d)\, \mu_o E\, \chi(\mu_o, \mu, \psi)], \qquad (2)$$

where δ is the Earth-Sun distance correction factor for Julian day d, E is the visible solar constant for NOAA-14 (511 W-m^{-2}sr^{-1}μm^{-1}), μ_o and μ are the cosines of the satellite viewing and solar zenith angles, and ψ is the relative azimuth angle. The narrowband bidirectional anisotropic reflectance factor χ for clear ocean, and cloudy scenes is defined by Minnis and Harrison (1984), while the Earth Radiation Budget Experiment broadband bidirectional model (Suttles et al., 1998) is used for clear snow or ice scenes.

There is onboard calibration of the three temperature channels of AVHRR, thereby eliminating the need to normalize the NOAA-12 with NOAA-14 temperatures. The IR (11-μm) window channel temperature T is converted to IR narrowband flux

$$M_{ir} = 1.97\, \pi\, B[T(\mu)] / \gamma(\mu), \qquad (3)$$

where B is the Planck function at 10.9 μm, T is the temperature, γ is the limb darkening function defined by

Month	ΔT_{34}	ΔT_{45}
MAY	8.2/1.7	1.47/0.45
JUNE	6.3/1.3	1.57/0.35
JULY	4.0/1.7	1.34/0.39

Table 1. Thresholds for cloud identification. Left number is the mean and the right is the standard deviation for all images for the month in K°.

Minnis and Harrison (1984) and the 1.97 factor accounts for the bandwidth.

3. SCENE IDENTIFICATION

Images from the first two weeks of each month were manually scene identified using a set of four thresholds that varied with image. Each pixel was classified as clear ocean, snow, or cloudy. The thresholds were determined for the following parameters: the VIS (0.65-μm) reflectance; T_4 (11-μm); ΔT_{34}, the difference of T_3 (3.7-μm) and T_4; and ΔT_{45}, the difference of T_4 and T_5 (12-μm). Over snow, a VIS threshold cannot be used to determine cloudy scenes because the surface and cloudy albedos are similar. Only the temperature thresholds are used to determine cloudy scenes. If ΔT_{34}, or ΔT_{45} exceeds the threshold, the pixel is cloudy. The latter is better for detecting cirrus, while the former is better to detect most other cloud types over snow. If T_4 exceeds the threshold, a warm cloud over snow is detected. This threshold is usually 273°K. This feature is mainly used in July. If the pixel is clear, a VIS albedo threshold of 0.06 determines whether the pixel is ocean or snow. Table 1 quantifies the some of the thresholds for the period.

Further scene identification is being developed to determine (cloud) shadow or lead pixels. Leads can also be seen in cloudy parts of the VIS image. It would be advantageous to automate the scene identification procedure. This requires an estimate of the reflected part of the channel-3 radiance as a function of viewing and illumination conditions. Preliminary analysis indicates that the bidirectional reflectance model is inadequate because the differences depend on orientation of the orbit relative to the SHEBA ice camp. Furthermore, diamond dust (very small airborne ice particles near the surface) may increase the ΔT_{34} signal in otherwise clear-sky conditions.

The 2-week mean cloud amounts were computed for each of the 0.5° latitude by 2° longitude regions defined by the domain. Cloud amount is defined as the number of cloudy pixels divided by the total number of pixels in the region. Cloud amounts were linearly interpolated in time to compute amore realistic time-averaged cloud amount. Figure 1 show the spatial distribution of the derived mean cloud amounts for the three time periods. The cloud amount for the region containing the SHEBA ship was compared to the 6-hourly SHEBA surface

Month	#	BIAS	RMS	SHEBA
MAY	15	-0.3	1.9	90.8/19.6
JUNE	28	0.5	15.5	78.2/29.0
JULY	16	5.3	10.1	84.4/25.4

Table 2. Mean SHEBA and AVHRR cloud amounts in %. BIAS is AVHRR - SHEBA. Last column contains means / standard deviations for all SHEBA cloud amounts.

observations that were reported in eighths. Only those AVHRR images taken within 1 hour of a surface observation were used. The results are shown in Table 2. The rms differences are half of the standard deviations for all ship observations and within one eighth, lending some confidence to the scene identification procedure.

4. NARROWBAND TO BROADBAND

Both the ERBE-scanner and AVHRR instruments were operating on NOAA-9 during June 1986. Average ERBE OLR and albedos and AVHRR albedos and IR radiances were matched on a 2.5°grid over the domain of 65°N to 75° and 130°W to 170°W. Scene identification as described above was applied to the AVHRR Global Coverage Data (GAC) 4-km resolution images. Only satellite view zenith angles less than 45° and solar zenith angles less than 84° were used. The regression follows the approach of Minnis et al. (1995).

The following equation resulting from the regression analyses is used to compute broadband albedos,

$$\alpha_b = -0.0130 + 0.8005\alpha_n - 0.0837\alpha_n^2 + 0.09 \ln(1/\mu_o). \quad (4)$$

The squared correlation coefficient is 0.91 and the rms difference between the ERBE and AVHRR-predicted albedos is 0.0361. Figure 2 shows the scatterplot for June 1986 albedo along with the regression fit for a range of solar zenith angles.

The regression equation for OLR from IR narrowband flux is

$$M_{lw} = -26.38 + 10.3M_{ir} - 0.08M_{ir}^2 - 0.11M_{ir} \ln(RH), \quad (5)$$

where RH is the National Center for Environmental Prediction (NCEP) column-weighted relative humidity (in percent) above the radiating surface. FIRE-ACE RH is estimated from the SHEBA soundings using only the standard levels in the NCEP product. The squared correlation coefficient is 0.88 and the rms difference is 5.81Wm^{-2}.

4. CLOUD FORCING

The AVHRR fluxes were binned in the same regions as cloud amount. The regions are 55-km x 55-km. The fluxes are interpolated in time using ERBE time-space

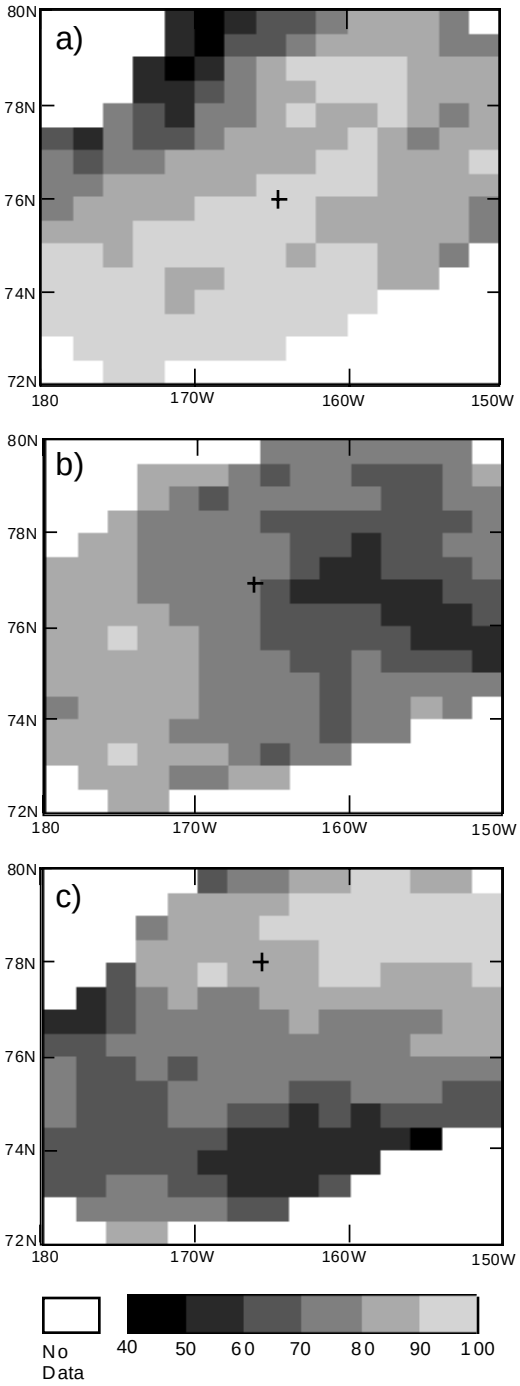

Fig. 1. AVHRR cloud amounts in % for a) May b) June and c) July. The + indicates the location of SHEBA.

averaging techniques (Young et. al. 1998) to minimize the effects of the AVHRR sampling patterns. The clear sky products only used measurements where the instantaneous clear amounts are greater than 10%. This is necessary to
shadows or three dimensional cloud effects due to the high solar zenith angles. Figure 4 shows the clear-sky

Month	#	OLR_{clr}	OLR	α_{clr}	α	CF
MAY	50	209.6	195.9	0.63	0.69	-10.0
JUNE	89	223.6	215.4	0.57	0.62	-19.4
JULY	73	230.4	214.6	0.51	0.57	-16.4

Table 3. Cloud forcing statistics over SHEBA. OLR and CF are in Wm^{-2}.

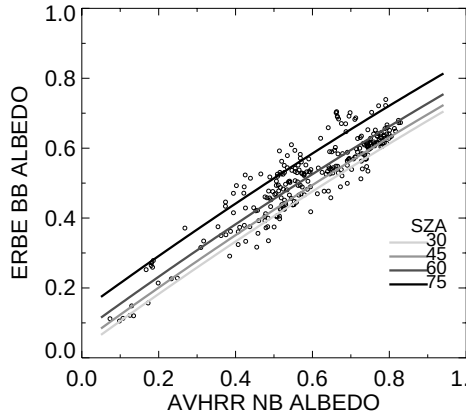

Fig. 2. Correlation of June 1986 NOAA-9 narrowband ERBE broadband albedos.

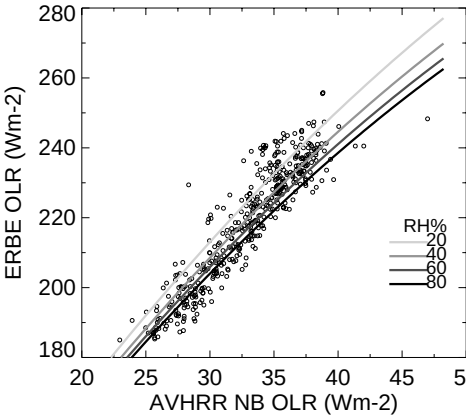

Fig. 3. Correlation of June 1986 AVHRR narrowband flux and ERBE broadband OLR.

albedo during the first 2 weeks of June 1998 when SHEBA observed the start of the ponding on the ice. The lower clear-sky albedos in the south indicate ponding, whereas the surface is mostly ice in the north.

The standard definitions of longwave (lw), shortwave (SW), and net cloud forcing (CF) are, respectively,

$$CF_{lw} = OLR_{clr} - OLR;\ CF_{sw} = S(\alpha_{clr} - \alpha);\ CF = CF_{lw} + CF_{sw}$$

where S is the mean incoming solar flux and α is the albedo. Table 3 shows the biweekly CF results over

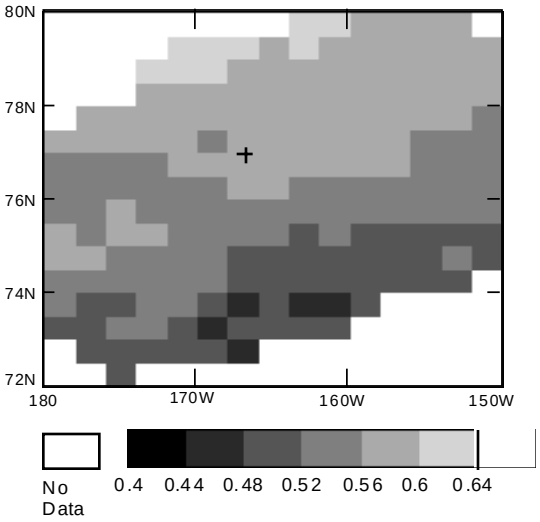

Fig. 4. June AVHRR clear sky albedo. The + indicates the location of SHEBA.

SHEBA. The cloudy albedos are greater than the clear albedos in the Arctic. The magnitude of the SW term is twice the LW term. The SW forcing is a function of the clear-sky albedo. A significant clearing event occurred during June. Figure 5 shows the spatial variation of CF. Diurnal variations of these parameters were also computed .

6. CONCLUDING REMARKS

The results presented here have shown a negative cloud forcing during spring and summer over the greater SHEBA domain. The small contrast between clear and cloudy scenes is found for both shortwave and longwave radiation. Apparently, the long daylight periods cause a net cooling by clouds during the summer. Possible errors in the cloud forcing product include the ERBE snow and overcast models used to interpolate over time, narrowband calibration, and the robustness of the narrowband to broadband relationship. The AVHRR derived albedos and OLR fluxes will be compared with the TSBR onboard the C-130 to validate the results. Additional periods will also be analyzed.

References

Minnis P. and E. F. Harrison, 1984: Diurnal variability of regional cloud and clear-sky radiative parameters derived from GOES data; Part III: November 1978 radiative parameters. J Climate Appl. Meteorol., **23**, 1032-1052.

___, , W. L. Smith, Jr., D. P. Garber, J. K. Ayers, and D. R. Doelling, 1995: Cloud properties derived from GOES-7 for Spring 1984 ARM Intensive Observing Period using Version 1.0.0 of ARM satellite data analysis program. NASA RP 1366, 58 pp.

Rao, C. R. N., and J. Chen, 1996: Post launch calibration of the visible and near-infrared channels of the Advanced Very High Resolution Radiometer on NOAA-14 spacecraft. Intl Jour. Remote Sens., **17**, 2743-2747.

Suttles, J. T., R. N. Green, P. Minnis, G. L. Smith, W. F. Staylor, B. A. Wielicki, I. J. Walker, D. F. Young, V. R. Taylor, and L. L. Stowe, 1988: Angular radiation models for Earth-atmosphere system: Volume I - Shortwave radiation. NASA RP 1184, 144 pp.

Young, D. Y., P. Minnis, D. R. Doelling, G. G. Gibson and T. Wong, 1988, Temporal Interpolation Methods for the Cloud s and the Earth's Radiant Energy System (CERES) Ecperiment. Journ. of Applied Meteorology, **37**, 572-590,

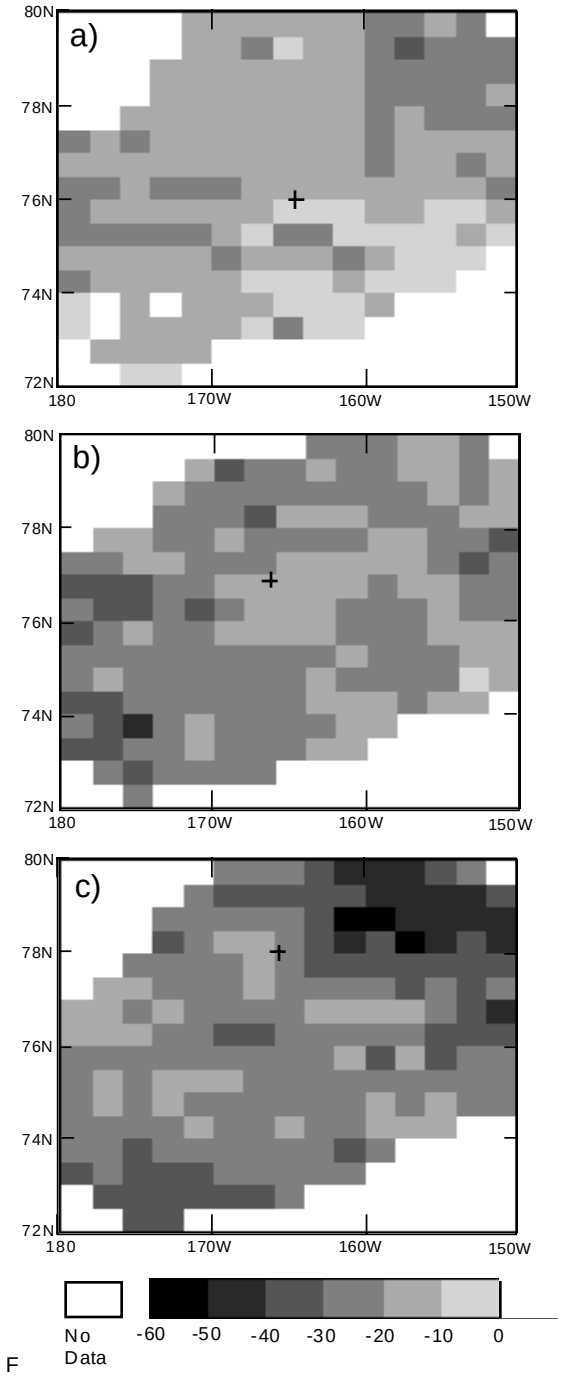

F

Fig. 5. AVHRR CF in Wm^{-2} for a) May b) June and c) July. The + indicates the location of SHEBA.